Astroparticle Physics 35 (2011) 201–210

Contents lists available at SciVerse ScienceDirect

Astroparticle Physics

journal homepage: www.elsevier.com/locate/astropart

A method for untriggered time-dependent searches for multiple flares from neutrino point sources

D. Góra [a,b,*], E. Bernardini [a], A.H. Cruz Silva [a]

[a] DESY, D-15735 Zeuthen, Germany
[b] Institute of Nuclear Physics PAN, ul. Radzikowskiego 152, 31-342 Cracow, Poland

ARTICLE INFO

Article history:
Received 11 April 2011
Received in revised form 21 July 2011
Accepted 28 July 2011
Available online 8 August 2011

Keywords:
Neutrino
Time-dependent searches
Neutrino experiments

ABSTRACT

A method for a time-dependent search for flaring astrophysical sources which can be potentially detected by large neutrino experiments is presented. The method uses a time-clustering algorithm combined with an unbinned likelihood procedure. By including in the likelihood function a signal term which describes the contribution of many small clusters of signal-like events, this method provides an effective way for looking for weak neutrino flares over different time-scales. The method is sensitive to an overall excess of events distributed over several flares which are not individually detectable. For standard cases (one flare) the discovery potential of the method is worse than a standard time-dependent point source analysis with unknown duration of the flare by a factor depending on the signal-to-background level. However, for flares sufficiently shorter than the total observation period, the method is more sensitive than a time-integrated analysis.

1. Introduction

The major aim of neutrino astrophysics is to contribute to the understanding of the origin of high energy cosmic rays. A point-like neutrino signal of cosmic origin would be an unambiguous signature of hadronic processes, unlike γ-rays which can also be created in leptonic processes. Neutrino telescopes are ideal instruments to monitor the sky and look for the origin of cosmic rays because they can be continuously operated. The detection of cosmic neutrinos is however very challenging because of their small interaction cross-section and because of a large background of atmospheric neutrinos. The cross-section for charge current neutrino interactions is about 10^{-34} cm^2 at an energy of 100 TeV [1]. Parallel measurements using neutrino and electromagnetic observations (the so-called "multi-messenger" approach) can increase the chance to discover the first neutrino signals by reducing the trial factor penalty arising from observation of multiple sky regions and over different time periods [2]. As an example, the significance of the observation of neutrinos can be enhanced by follow-up observations with optical telescopes. Such a system has been set up for IceCube [3,4] and ANTARES [5]. It looks for spatial and temporal coincidences between neutrino candidates in the data and sends corresponding alerts to robotic optical telescopes arrays that perform follow-up observations over several weeks. In the future, both collaborations plan to extended their follow-up programs to other instruments, such as the high energy γ-ray telescope MAGIC [6] and Fermi satellite [5]. In a longer term perspective, the multi-messenger approach also aims at providing a scheme for a phenomenological interpretation of the first possible detections. The search of occasional flares with a high-energy neutrino telescope is motivated by the high variability which characterizes the electromagnetic emission of many neutrino candidate sources. Resent results obtained by the IceCube collaboration [7] indicate that high-energy neutrino telescopes have reached a sensitivity to neutrino fluxes which is comparable to the observed high energy *gamma*-ray fluxes of Blazars in the brightest states (e.g. the flares of Markarian 501 in 1997 [8], Markarian 421 in 2000/2001 [9] and PKS 2155–304 in 2006 [10]). With the assumption that the possibly associated neutrino emission would be characterized by a flux enhancement comparable to what is observed in *gamma*-rays in such states, neutrino flares could be extracted from the sample of neutrino-like events with a reasonable significance.

These astrophysical neutrinos can be searched for in several ways. One of the methods for a neutrino point source search is to look for events coming from a restricted angular region, which could be identified with a known astrophysical object. Finding neutrino point sources in the sky means to locate an excess of events from a particular direction over the background of atmospheric neutrinos and muons. These events might present additional features that distinguish them from background, for example a different energy spectrum or time structure. For sources which manifest

* Corresponding author at: Institute of Nuclear Physics PAN, ul. Radzikowskiego 152, 31-342 Cracow, Poland. Tel.: + 48 12 6628348; fax: + 48 12 6628012.
E-mail address: Dariusz.Gora@ifj.edu.pl (D. Góra).

0927-6505/$ - see front matter © 2011 Elsevier B.V. All rights reserved.
doi:10.1016/j.astropartphys.2011.07.007

large time variations in the emitted electromagnetic radiation, the signal-to-noise ratio can be increased by testing smaller time windows around the flare (a time-dependent search). In principle there are two approaches to neutrino time-dependent searches:

- **Triggered flare search**: Looking directly for photon-neutrino correlations using specific source lightcurves from Multi-Wave-Length (MWL) observations [11].
- **Untriggered flare search**: A generalized search (MWL data) for neutrino flares, motivated but not associated with MWL observations, which are scarce and not available for all sources during complete periods. In addition, there could be a time lag between observed photon flares and the associated neutrino flares. In the extreme cases high energy photons could be entirely absorbed during periods of the highest photon production in the source [12]. This approach however entails a higher trial factor penalty than triggered flare searches. As a merit, neutrino flares which are not accompanied by observed electromagnetic counter parts are not automatically excluded. This approach is also less dependent on models for the correlation between the neutrino and the electromagnetic emission and not dependent on the availability of multi-wavelength information.

Here we develop a method that is well suited for an intermediate approach in which "periods of interest" can be a priori selected on the basis of multiwavelength data. The neutrino sample can then be scanned looking for significant structures, in a way which is less dependent on models predicting different correlations with a given wavelength.

An untriggered unbinned flare search was first developed and applied to IceCube data, using a compact list of pre-defined source directions [7]. A time-clustering algorithm [7,13], and the unbinned maximum likelihood method [14,16] are the basis of this analysis. Such a method finds the most significant flare in a long period. The number of trials coming from all combinations of event times is increased, reducing the significance. However, for flares sufficiently shorter than the total observation period, the time clustering algorithm is more sensitive than a time-integrated analysis.

In this paper, we propose an extension of the method described in [7]. By including in the likelihood a signal term which describes the contribution of many small clusters of signal-like events, our algorithm can extract not only the most significant flare, but also less significant clusters of events distributed over weak flares. These weaker flares could be separated by any distance in time and will be very difficult to detect or even cannot be detected with other methods [14,16].

The paper is structured as follows. The algorithm is described in Section 2. In Section 3 we apply the method to a simulated neutrino search for one flare and a few weak flares separated in time. A short discussion about the algorithm performance is presented in Section 4. Conclusions are given in Section 5.

2. The algorithm

In this section, we first describe the time-clustering algorithm, then we shortly recall the unbinned maximum likelihood method [14] and finally we propose our new algorithm.

2.1. The time-clustering algorithm

The time clustering algorithm [7] selects the most significant cluster of events in time and returns the mean time and width of the corresponding flare. The basic idea is shown in Fig. 1. In a first step, the method selects the most promising flare candidates over

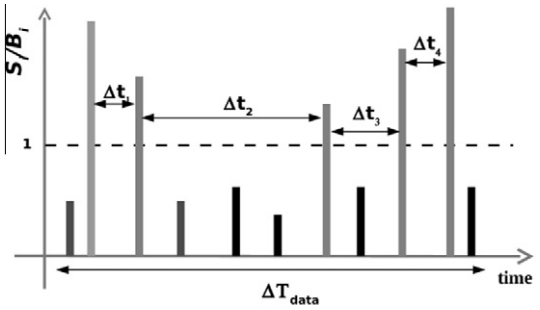

Fig. 1. The basic idea of the time clustering procedure. The signal-like events are extracted out of a data sample and then sorted in time. Each combination of such event pairs defines a possible flare time window, which is then tested with a maximum likelihood method.

different time windows (Δt_j), which are given by the combination of the times of signal-like events from the analyzed data set. A signal-like event is defined as having $S_i/B_i > 1$, where S_i and B_i is the background and the signal Probability Density Function (PDF) as defined for the time-integrated method [14].[1] Each combinations of these event times defines the start and end time ($t_j^{\min}$ and $t_j^{\max}$) of a candidate flare time window (Δt_j). For each Δt_j, a significance parameter (the test statistic) TS_j is then calculated as defined in [14]. Larger values of TS_j correspond to data less compatible with the null hypothesis (i.e. zero expected signal events in the data sample tested). Finally, the algorithm returns the best TS_j, $\mathrm{TS}_{\max}$, corresponding to the most significant time window over the entire data period analyzed.

2.2. The unbinned maximum likelihood method

The unbinned maximum likelihood method [14] defines the test statistic parameter by:

$$\mathrm{TS}_j = -2\log\left[\frac{\mathcal{L}(\vec{x}_s, n_s = 0)}{\mathcal{L}(\vec{x}_s, \hat{n}_s, \hat{\gamma}_s)}\right], \tag{1}$$

where $\vec{x}_s$ is the source location, $\hat{n}_s$ and $\hat{\gamma}_s$ are the best estimates of the number of signal events and source spectral index, respectively, which are found by maximizing the likelihood $\mathcal{L}$:

$$\mathcal{L}(n_s, \gamma, \Delta t_j) = \prod_{i=1}^{N}\left(\frac{n_s}{N}S_i + \left(1 - \frac{n_s}{N}\right)B_i\right), \tag{2}$$

where N is the number of all events in the data sample.

The background PDF is given by:

$$B_i = P_i^{\mathrm{space}}(\theta_i, \phi_i)P_i^{\mathrm{energy}}(E_i, \theta_i)P_i^{\mathrm{time}}(t_i, \theta_i), \tag{3}$$

where P_i^{space} describes the space distribution of events at a given region of the sky with the solid angle $d\Omega$, P_i^{energy} is the energy distribution and P_i^{time} describes the background time distribution. These PDFs can be calculated purely from data. In general, due to analysis cuts, Earth absorption effects and the detector geometry, the spatial probability P_i^{space} and the energy probability P_i^{energy} depend on zenith, θ_i, and azimuth, ϕ_i.

The time probability P^{time} is defined by:

$$P_i^{\mathrm{time}}(t_i, \theta_i) = \frac{1}{\Delta T_{\mathrm{data}}}, \tag{4}$$

where ΔT_{data} is a normalization constant for the whole data taking period.

[1] To calculate the ratio, $S_i/B_i > 1$, only the spatial and energy terms in the PDFs are included.

The properties of neutrino signal events are taken from a dedicated Monte Carlo (MC) signal simulations.

The signal PDF, S_i is given by:

$$S_i = P_i^{\text{space}}(|\vec{x}_i - \vec{x}_s|, \sigma_i) P_i^{\text{energy}}(E_i, \theta_i, \gamma_s) P_i^{\text{time}}, \tag{5}$$

where the spatial probability P_i^{space} is a Gaussian function of $|\vec{x}_i - \vec{x}_s|$, the space angular difference between the source location $\vec{x}_s$ and each event's reconstructed direction $\vec{x}_i$, and σ_i the angular error estimate of the reconstructed track. The energy probability P_i^{energy}, constructed from neutrino signal simulation, is a function of the event energy estimator E_i, the zenith coordinate θ_i, and the assumed energy spectral index of the source γ_s (such that $\frac{dN}{dE} \sim E^{-\gamma_s}$). P_i^{time} is the time probability which generally is a constant value (i.e. taken to be uniform in time) if no flare structure is assumed. For each time window tested $\left(\Delta t_j = t_j^{\max} - t_j^{\min}\right)$, the time probability is given by:

$$P_i^{\text{time}} = \frac{H\left(t_j^{\max} - t_i\right) H\left(t_i - t_j^{\min}\right)}{\Delta t_j}, \tag{6}$$

where t_i is the arrival time of the ith event and H is the Heaviside step function [15]. Note, that by using this definition for the time probability in the likelihood $\mathcal{L}$, we count only events which fall inside the current time window Δt_j (i.e. the signal PDF S_i is zero outside the selected time window).

As shown in [16] the unbinned likelihood method will preferentially find shorter flares, making it less powerful for flares of durations longer than roughly one day. The solution to this problem is to use a marginalization term $\left(\frac{\Delta t_j}{\Delta T_{\text{data}}}\right)$ in the likelihood $\mathcal{L}$ [16]. This gives a more uniform exposure to find flares of different widths and leads to a redefinition of the test statistic:

$$\text{TS}_j|_{\Delta t_j} = -2 \log \left[\frac{\Delta T_{\text{data}}}{\Delta t_j} \times \frac{\mathcal{L}(\vec{x}_s, n_s = 0)}{\mathcal{L}(\vec{x}_s, \hat{n}_s, \hat{\gamma}_s)} \right]. \tag{7}$$

2.3. A method to search for multiple flares

We propose here some extensions to the above mentioned procedures to identify a series of weak flares by incorporating this information into the likelihood function. This is done by restricting the search to doublets of signal-like events, and using the value of the test-statistic of these individual flare candidates as their weights in a stacking-like calculation of the global maximum likelihood.

First, we extract all *consecutive doublets* that can be formed out of all signal-like events ($S_i/B_i > 1$) over the entire data taking period ΔT_{data}. This step serves to isolate all possible (and smallest) time windows that compose the signal contribution in the tested data sample (the total number being M). We call these time windows "data segments". Note, that by construction, there could be a certain degree of overlap between different data segments if larger data segment multiplicity will be studied, see Fig. 2 Top. The choice of doublets is physics-motivated, because for a neutrino detector like IceCube, the signal expectation is not much more than a few signal neutrinos per year from the strongest astrophysical sources [17]. Moreover, we focus on weak multiple flares.

Then for each time window Δt_j a minimization of $\log(\mathcal{L})$ as defined in Eq. (2) is performed, with n_s and γ_s as free parameters, and the individual test statistic $\text{TS}_j|_{\Delta t_j}$ is calculated. This step serves to estimate the possible signal contribution in each data segment. All time windows are then sorted according to $\text{TS}_j|_{\Delta t_j}$, as it is shown in Fig. 2 (Middle). Some of these data segments will contain real signal events and some of them are likely due to background fluctuations. Our aim is to extract the optimal (best suited) number of data segments (M_{opt}) which compose the total signal contribution injected in the overall period ΔT_{data}.

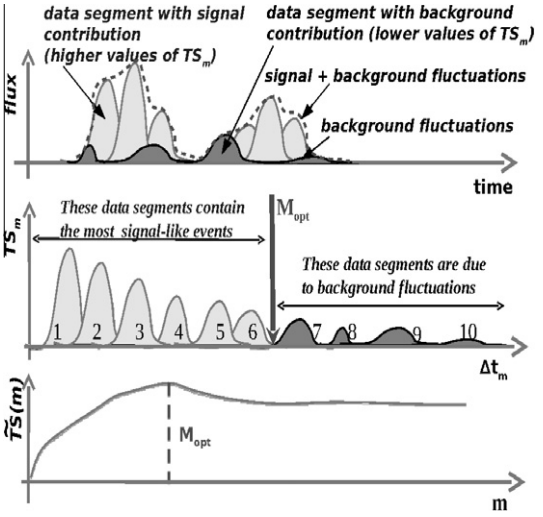

Fig. 2. Sketch of the flare stacking procedure. Top: A data set is divided into segments being defined as in Fig. 1. Some of these segment will include signal contribution, others background fluctuations only; Middle: sorted values of the test statistic for each data segment from a maximization of the likelihood in Eq. (2) as a function of the data segment index m. Bottom: Evolution of the test statistic from a maximization of the likelihood in Eq. (8) as a function of the number of data segments being stacked following Eq. (9). The maximum value of this parameters defines the optimal number of data segments to be stacked M_{opt}.

For this purpose, we propose a modification of the single-source likelihood function (Eq. (2)) by including a signal term $(S_i^{\text{tot}}(m))$ describing the contribution of each data segment:

$$\tilde{\mathcal{L}}(n_s, \gamma, m) = \prod_{i=1}^{N} \left(\frac{n_s}{N} S_i^{\text{tot}}(m) + \left(1 - \frac{n_s}{N}\right) B_i \right), \tag{8}$$

where m is the number of data segments into which the overall signal contribution can be decomposed (a free parameter $m \leqslant M$) and N is the total number of events in the time period ΔT_{data}.

In other words, in order to include the contribution to the signal from multiple flares, the one-source signal term S_i is being replaced by the sum of signal sub-terms over m data-segments:

$$S_i \to S_i^{\text{tot}}(m) = \frac{\sum_{j=1}^{m} W^j \times S_i^j(|\vec{x}_i - \vec{x}_s|, E_i, \gamma, \Delta t_j)}{\sum_{j=1}^{m} W^j}, \tag{9}$$

where W^j is a weight which describes the strength (significance) of the doublet contained in each data segment. This weight should be proportional to the expected number of neutrino events seen in the detector. As we will show later the test statistic is quite well correlated with the true number of injected signal events. Thus we take $W^j = \text{TS}_j|_{\Delta t_j}$.

The likelihood given in Eq. (8) in combination with Eq. (9) is usually used in stacking searches for different types of astrophysical point sources [18], but here the individual sources are data segments of the signal-like events found in the data from the same object. The stacking method uses the fact that signal and background increase differently when observations for multiple sources (or flares) are being added. Stacking multiple flares can therefore suppress the overall background and hence can increase the signal sensitivity.

In order to estimate the optimal number of data segments M_{opt} for a given number of m segments (starting from $m = 1$) we minimize the $\log(\tilde{\mathcal{L}}(n_s, \gamma, m))$ with n_s and γ_s as free parameters. The minimization returns the best estimates for the number of signal events $\hat{n}_s$ and for the spectral index of the source $\hat{\gamma}_s$, and the "global" test statistic is calculated from:

$$\widetilde{\mathrm{TS}}(m) = -2\log\left[\frac{\tilde{\mathcal{L}}(\vec{x}_s, n_s = 0)}{\tilde{\mathcal{L}}(\vec{x}_s, \hat{n}_s, \hat{\gamma}_s, m)}\right]. \quad (10)$$

Then, the optimal number of data segments to be stacked (M_{opt}) is chosen according to the maximum of $\widetilde{\mathrm{TS}}(m)$ (see Fig. 2 Bottom). As a result, the following important parameters are extracted:

- M_{opt}: the optimal number of segments which compose the signal contribution over the time ΔT_{data}. The optimal set could be either subsequent in time, forming one significant cluster of events (one flare) for a given source location, or theses segments can be distributed among a few (sometimes less significant) flares separated in time. This is shown in Fig. 2 (Top).
- $\hat{n}_s$: the total number of expected signal events summed over the M_{opt} individual segments.
- $\hat{\gamma}_s$: the spectral index of the source (the flare), assumed to be the same for each M_{opt} segments.
- $\widetilde{\mathrm{TS}}(M_{\mathrm{opt}})$: the maximum value of the test statistic calculated with the modified likelihood function of Eq. (10).
- $\Delta T(M_{\mathrm{opt}})$: the flare duration calculated for M_{opt} segments. This is here defined as the time between the start time of the first data segment and the end time of the last data segment.

The overall significance of the optimal configuration M_{opt} can be determined using MC simulations by applying the same procedure to a large number of simulated data samples. This will automatically account for effects of trial factors. The trial factors arise from testing different time windows for the same source direction. In order to represent a background-only observation, the properties of the data events (e.g. zenith, azimuth, time, reconstruction error and energy estimator) are sampled from their distributions. Data of neutrino experiments with a signal flux can be simulated by injecting signal events on top of the background data.

3. Results

The method described in Section 2 has been applied to 10,000 MC background samples (scrambled sky maps). Background events were randomly chosen reproducing realistic PDF's (energy, angular resolution) extracted from [17]. By using these distributions, simulations are performed for conditions of the IceCube detector. IceCube is km^3 scale neutrino detector at the south pole sensitive to TeV neutrinos [17]. More precisely, the number of background events in a given declination band $\left(n_{\mathrm{bg}}^{\mathrm{band}}\right)$ is estimated from $n_{\mathrm{bg}}^{\mathrm{band}} = n_{\mathrm{bg}} \times \frac{A_{\mathrm{band}}}{A_{\mathrm{bin}}} \times \frac{\Delta T_{\mathrm{data}}}{375.5}$, where n_{bg} is the number of background events in a bin, 375.5 the live time of the data taking period of IceCube detector with 40-string configuration and A_{band} and A_{bin} are the solid angles of the band and bin, respectively. Assuming $n_{\mathrm{bg}} = 2.5$ background events for declination $\delta = 15^\circ$ as in [17] and $\Delta T_{\mathrm{data}} = 40$ days we are left with 355 events distributed in a declination band of size $\pm 6^\circ$. The angular reconstruction error σ_i of each event was generated based on the cumulative spread function from [17] with a median resolution of about 0.8° and assuming that σ_i does not depend on the energy of the reconstructed event. This assumption in general may not be true, but it will not affect the results of this test. The same number of scrambled maps were generated for signal events injected on top of the background (MC background plus signal simulations). A neutrino point source at declination 15° was considered. For the IceCube detector the sensitivity to a point E^{-2} flux of muon neutrino depends on declination of the source (zenith angle) [17]. For the northern sky, the expected sensitivity has a flat minimum for a declination of about 10°. Thus, simulation performed in this work (source with declination 15°) corresponds to the declination range, where the detector like IceCube has the best sensitivity for neutrinos. For the southern sky,

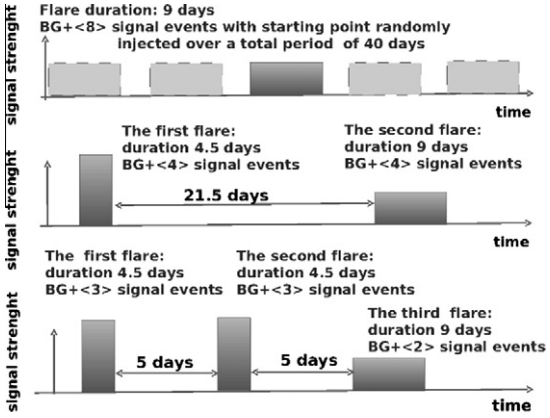

Fig. 3. Sketch of the three examples discussed in this work from top i.e. one flare (Example 1) two individual flares (Example 2) and three weak flares separated in time (Example 3).

the neutrino sensitivity also depends on declination (zenith angle), but due to a much higher background level from atmospheric muons, the sensitivity is more than one order of magnitude worse than the sensitivity for the northern sky. Signal events were injected around this declination δ_s along a band $\delta_s - 6^\circ < \Delta_s < \delta_s + 6^\circ$[2] and with azimuth randomly chosen from 0° to 360°. Individual event directions were smeared according to the Point Spread Function (PSF) from [17] with a median angular resolution of about 0.8°. We simulate signal strengths following Poisson statistics with mean values of 4, 8, 9 and 12 signal events. The energy PDF follows what was found for an E^{-2} energy spectrum in [17]. For each MC signal sample (scrambled sky map), signal events were randomly injected inside a time window defined by various flare durations, in the range from 0.01 day to 30 days. The most of the results presented in this paper was obtained considering a total period of $\Delta T_{\mathrm{data}} = 40$ days. This is motivated by the fact that an obvious application of this method is to test periods of interests, preselected with the help of multi-wavelengths data.

We tested the method for the three following cases which are also illustrated in Fig. 3.

Example 1. Signal events (with Poisson-mean = 8) are injected inside a 9 days time window. The starting point of the flare is randomly chosen over a data taking period ΔT_{data} of 40 days. An example of a physics case corresponding to this configuration is the reported γ-ray flare from the Crab Nebula [19–21]. Note, that this case would correspond to a rather "strong" flare. As we can see for example from [16], the number of events required for the discovery of such a flare is larger than seven in case of a search with an unknown burst duration.

Example 2. The total number of signal events (Poisson-mean = 8) is the same as in Example 1, but individual events are injected over two time windows of duration 4.5 and 9 days, respectively and 22 days apart. The average number of injected signal events is the same for each flare (Poisson-mean = 4). The expected number of events required for the discovery depends on the flare duration and it is smaller for the flare with shortest duration. In other words we can think of this example as a case with a "strong" flare and one weaker flare. These two flares are separated in time, but they can also be treated as one long period of enhanced emission with a

[2] Events outside this band hardly contribute to the signal PDF since they are too far away from the source compared to the point spread function of [17].

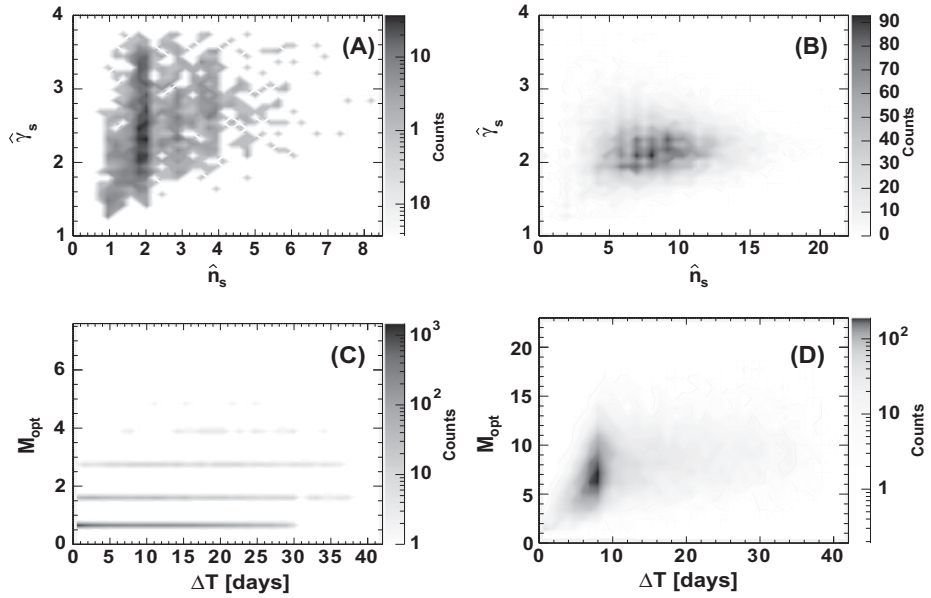

Fig. 4. (A), (B) Distribution of the best fit values for the number of signal events $\hat{n}_s$ and the source spectral index $\hat{\gamma}_s$ and their correlations for background-only simulations (Left) and with 8 (Poisson-mean) signal events injected on the top of the background (Right) for a source at declination 15°. (C), (D) The optimal number of data segments $M_{\rm opt}$ as a function of the duration of the flare ΔT (i.e. the maximum time difference between any data segments yielding the best fit configuration $M_{\rm opt}$).

duration about of 35 days. Standard point source search methods applied to this case will find only the strongest flare i.e. the first one. This is because standard methods use the one-source likelihood function given by Eq. (2) and can look only for a minimum corresponding to the most significant cluster of events from a given source location.

Example 3. The total number of signal events (Poisson mean = 8) is the same as in previous examples, but individual events are injected over three time windows with duration of 4.5 days, 4.5 days and 9 days, respectively. Each flare is simulated with a similar strength with Poisson-mean 3, 3 and 2, respectively. This example describes three "weak" flares. Note that the number of events required to claim discovery for each of them at a 5σ level is larger than four, as we can see from [16].[3] In other words such individual weak flares cannot be found at a 5σ level by the standard point sources search methods.

3.1. Example 1: one flare

In Fig. 4 the distribution of the most important parameters i.e. the number of signal events $\hat{n}_s$, the spectral index $\hat{\gamma}_s$ and the optimal number of data segments (i.e. signal-like doublets) $M_{\rm opt}$ and their correlations as obtained by MC simulations are presented for the background-only simulations and the background plus signal cases. The number of injected signal events follows a Poisson distribution with a mean of 8. Events are injected over a time window of 9 days duration. The pure background case illustrates how signal-like flares can be mimicked by pairs of events (sometimes also triplets) distributed over very short time windows with durations of less than a day. The signal plus background plots show that the proposed method finds the right flare i.e. it recovers the true values of the spectral index (2), the number of injected signal events (Poisson-mean 8 events) and the flare duration [4] (9 days). In addition, the flare can be decomposed into about eight data segments, see Fig. 4 (D).

In Fig. 5 (A) the correlation of the global test statistic $\widetilde{\rm TS}(M_{\rm opt})$ as a function of the number of injected signal events n_s (MC) is shown. The solid line represents a linear fit to the mean values of the test statistic calculated for a fixed number of injected signal events. A linear correlation is found between the test statistic and number of injected signal events. This justifies using the test statistic as a weight in the modified likelihood $\tilde{\mathcal{L}}$ of Eq. (9). We also checked the results obtained when all weights are fixed to one as well as to the square of the test statistic. We find that such modifications lead to slightly worse results i.e. we observed a 5%–10% worse agreement between the true and the estimated values of $\hat{n}_s$ and $\hat{\gamma}_s$.

In Fig. 5 (B) the number of signal events is shown as a function of the optimal number ($M_{\rm opt}$) of data segments which compose the flare. As expected, the number of signal events increases when more segments are being added. The distribution shows a maximum corresponding to the true number of injected signal events (the true Poisson-mean of 8). The inset in Fig. 5 (B) shows the Gaussian fit to the estimated number of signal events, $\hat{n}_s$ with a mean value of 8.2, which is good agreement with the true value at a level of about 2.5%.

The proposed algorithm can therefore recover the most important parameters characterizing flares, like the duration, the source spectral index and the number of injected signal events with uncertainties not larger than a few percent. In other words the proposed algorithm can "decompose" the flare into small data segments which contain signal-like doublets and can effectively reject background events from the entire data period.

[3] In this work we injected signal events according to a uniform distribution while in [16] a Gaussian distribution was considered. While a general comparison is still possible in some cases the exact numerical results are different. The duration of a time window, for example, is somewhat different. For a uniform distribution with non zero values in the interval Δt the standard deviation is defined according to $\sigma = \Delta t/\sqrt{12}$ with σ denoting the standard deviation of the Gaussian distribution. Thus 4.5 and 9 days width of the flare corresponds to $\sigma_t \simeq \sigma$ about 1.3 and 2.6 days or to 0.0035 and 0.0070 year, respectively. Thus for the flare with a Gaussian mean time $\sigma_t = 0.0035$ we need about four events for discovery using the method labeled by "Assumed Burst Time (Energy)" in Fig. 4 of [16].

[4] The exact duration of the flare can be slightly less since the signal events were randomly injected inside the 9 days time window.

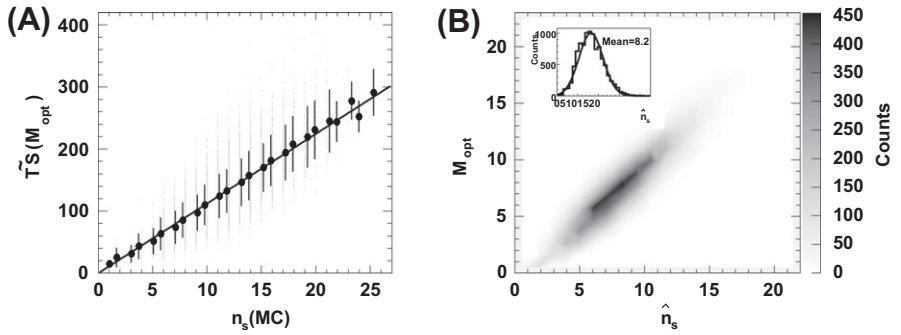

Fig. 5. (A) Correlation of the test statistic and the true number of injected signal events. The points which form vertical dashed lines describe the results of simulation of 10,000 data sets when signal events were injected according to Poisson distribution with a Poisson mean ranging from 4 up to 16 i.e. around the true number of injected signal events (8). The solid line represents a linear fit to data. Full circles correspond to an average value of the test statistic for a fixed number of injected signal events. (B) The optimal number of doublets which compose the flare with 9 days duration as a function of the average number of expected signal events. The inset shows the distribution of the best fit values of the number of signal events which can be well fitted with a Gaussian.

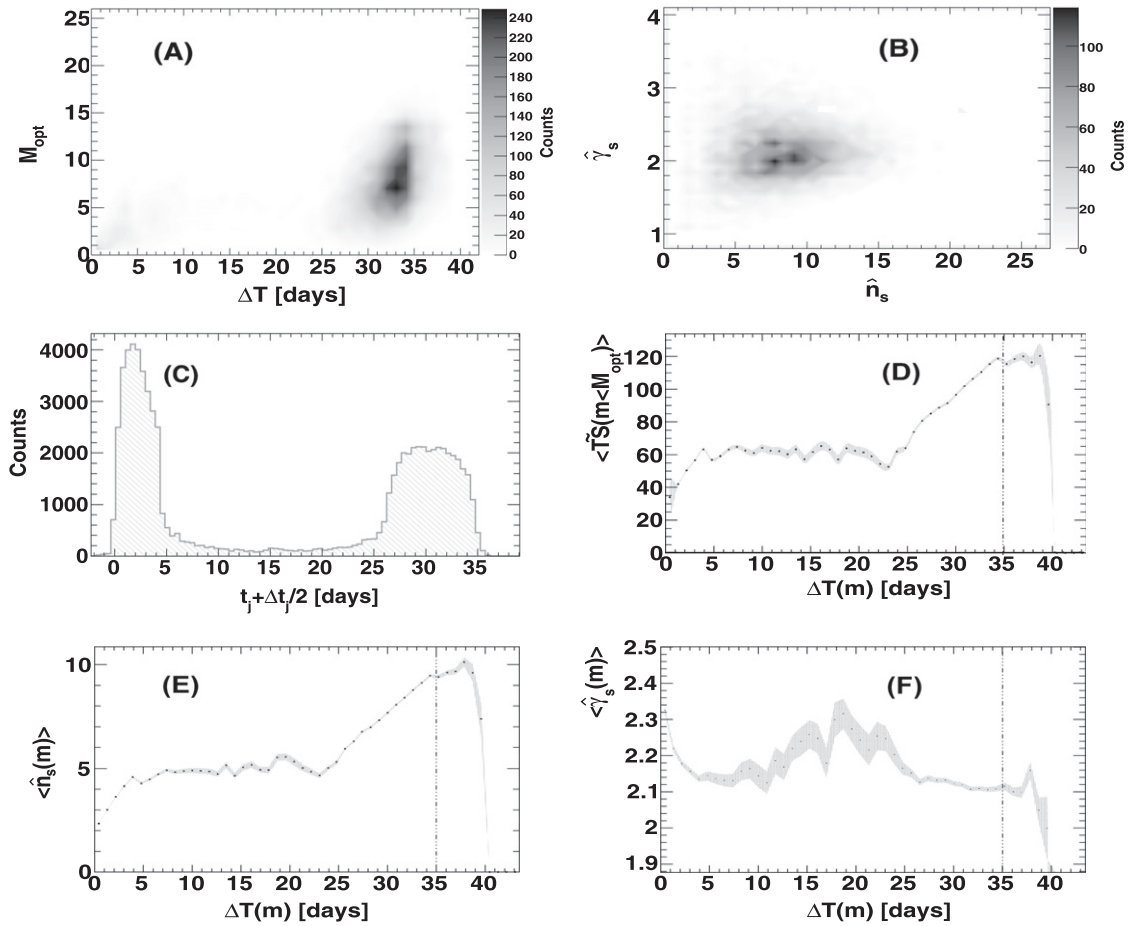

Fig. 6. Example 2: Results of the search for two individual flares separated in time using the method presented in this work. (A) Distribution of the optimal number of doublets (M_{opt}) as a function of the total flare duration ΔT; (B) The spectral index versus the expected number of signal events; (C) The mean time of each data segment; (D), (E), and (F) The distribution of $< \widetilde{TS}(m) >$, $< \hat{n}_s(m) >$ and spectral index $< \hat{\gamma}_s(m) >$ as a function of the flare duration $\Delta T(m)$. Also shown are $1-\sigma$ ranges. The vertical dashed line indicates the overall period of enhanced emission (35 days). See the text for more details.

3.2. Example 2: two flares separated in time

In Fig. 6 (A) we show the distribution of the optimal number of data segments M_{opt} as a function of the corresponding flare duration ΔT as defined in Section 2.3. In Fig. 6 (B) the best fit spectral index $\hat{\gamma}_s$ is shown as a function of the estimated number of signal events $\hat{n}_s$. Also in this case the proposed algorithm recovers the overall flare duration, the source spectral index and the number of injected signal events. However, for this particular case, the differences between the true and the estimated values of the physics parameters obtained from the minimization are slightly worse (about 5%). This is because for the larger flare durations we should expect a larger contamination of background events.

In Fig. 6 (C) the distribution of the mean time $T_{0,j} = t_j + \Delta t_j/2$ calculated for each (jth) signal-like doublet is shown. An accumulation of signal-like doublets for a time period below 5 days and

between 25 and 35 days is visible, corresponding to the first and the second flare, respectively. The proposed algorithm can therefore find not only the most significant flare, but also the weaker one separated in time. Such a flare would not be detected by other existing methods (like [16]).

By repeating the minimization with the modified likelihood $\tilde{\mathcal{L}}$ for a fixed number of m data segments *sorted in time* (starting from $m = 1$ and ending with $m = M_{\rm opt}$), we can get more information about the "internal" structure of the flare. For example, in Fig. 6 (D) changes of the global test statistic as a function of the flare duration $\Delta T(m)$ [5] calculated for $m < M_{\rm opt}$ data segments is shown. The test statistic increases when more segments are added in time, but finally reaches a saturation for the time corresponding to the overall period of enhancement emission (35 days). This behavior is strongly correlated with the distribution presented in Fig. 6 (C). For the first flare (below 5 days) and second flare (from 25 to 35 days) the increase of the global test statistic in time is much larger than during the period corresponding to the 22 days time gap. During this last period larger variations can also be observed, which is an indication for background fluctuations. A similar behavior is seen for the average number of signal events $< \hat{n}_s(m) >$ as a function of the flare duration (Fig. 6 (E)). Note that both distributions presented in Fig. 6 (D) and (E) are averaged over different MC realizations.

For completeness, Fig. 6 (F) shows the average spectral index $< \hat{\gamma}_s(m) >$ for a large number of different MC realizations as a function of time. The average best fit spectral index is about 2.2 and differs by about 8.5% from the true value ($\gamma_s = 2$). Similarly to the previous distributions, the fluctuations of the spectral index are strongly reduced during the periods corresponding to the injected signal. The effect is particularly visible for the second flare, between 25 days up to 35 days.

We conclude that the proposed algorithm can recover the global parameters describing the flares and provide additional information about the time development, their duration and the number of signal events per individual flare, even when they alone are below the threshold for detection.

3.3. Example 3: three weak flares separated in time

In Fig. 7 we show the results of simulations for three individual weak flares.

Fig. 7 (A) and (B) show that also in this case the method can recover the true values of the spectral index ($\gamma = 2$), the mean number of injected signal events (8) and the total flare duration (28 days). In addition, the overall signal injection can be decomposed into about 8 data segments (doublets).

Sorting these data segments in time we obtain the distribution *of individual flares* in time as shown in Fig. 7 (C). Three flares can be clearly distinguished, with a duration of about 5, 5 and 10 days, respectively.

The average value of the test statistic and the average number of signal events from the best fit (of the likelihood $\tilde{\mathcal{L}}$) is presented in Fig. 7 (D) and (E). We observe a similar behavior as in the Example 2. However, due to a smaller time gap between individual flares, a factor 4 smaller than for the flares studied in the Example 2, the structures are less pronounced. Note that the distributions presented in Fig. 7 (D) and (E) start to saturate at a point corresponding to the overall period of enhancement emission (above 28 days).

Finally, in Fig. 7 (F) the average spectral index $< \hat{\gamma}_s(m) >$ as a function of time is shown. The source spectral index has a value of about 2.2 and differs by about 10% from the true value ($\gamma_s = 2$). Fluctuations of the spectral index also increase for times greater than the total flare duration (above 28 days).

This example demonstrates that the proposed algorithm can find a few weak flares separated in time.

3.4. The flare with red-noise power density spectrum

Active Galactic Nuclei show strong variability that can be seen in the observed *X*-ray lightcurves [22]. The power density spectrum $S(f)$, defined as the distribution of power as a function of frequency (f), of these variations is a power law-like continuum with steep slope and in a some range of frequencies can be reasonably described by $S(f) \sim \frac{1}{f^{\alpha}}$, where α is a power-law index. Processes with steep power spectra like this are known as *red-noise* [23].

In order to show that the proposed algorithm works also for such cases, we also have performed simulations, when signal events were injected according to red-noise power density spectrum. The red-noise distribution of signal events were produced by an algorithm, detailed in [24]. This algorithm radomizes both phase and amplitude of an underlying power-law spectrum and then inverse Fourier transforms it into the time domain to create lightcurves.

In Fig. 8 results of calculation for 20 signal events injected according to the power density spectrum with $\alpha = 2$ are presented. In this case 10,000 simulated data sets are generated and signal events are injected inside a 20 days time window. As we can see from Fig. 8 (A), where the mean time of data segments is shown, the distribution have a typical behaviour seen for lightcurve with red noise power density spectrum i.e. the mean of noise level is not constant in time. Fig. 8 (B), (C) and (D) show that also in this case the method can recover the total flare duration (20 days), the number of injected signal events (20) and the true values of the spectral index ($\gamma \sim 2$). However comparing to previous examples the structures of the flare are less pronounced.

4. Performance of the method

In this section we calculate the number of events needed for discovery (i.e. the discovery potential) for the cases of Examples 1–3 and for different flares durations ΔT and overall data periods $\Delta T_{\rm data}$. The discovery potential is defined as the average number of signal events required to achieve a p-value less than 2.87×10^{-7} (one-sided 5σ) in 50% of the trials. The comparison below gives us an idea about the performance of the proposed method and its limitations.

In case of Example 3 we simulated three individual weak flares. Each flare cannot be individually detected at a 5σ level by using the standard point source search methods. In principle, if all events could be injected into a single flare of duration about 28 days ($\sigma_t \simeq 0.02$ year) the algorithm proposed in [16] would yield a discovery. For a flare of such a duration, more than about 7 events are needed for discovery at a 5σ level using the method labeled by Assumed Burst Time (Energy) in Fig. 4 of [16]. However, the flare will be found only if these 7 events will form *one cluster of events compact in time*. This is because the unbinned maximum likelihood method with a single-source likelihood function can only search for a maximum which corresponds to the most significant flare (cluster of events) from a point source. This is certainly not the case for this example, where 8 events are distributed among three individual and well separated flares. Thus, such a structure cannot be detected at 5σ level by the standard method.

In Fig. 9 we show the distribution of the global test statistic $\widetilde{\rm TS}(M_{\rm opt})$ for MC background-only simulations (A) and for MC background-plus-signal simulations (B), with signal events distributed

[5] For a fixed number m of data segments, the flare duration is defined as the time between the start time of the first in time data segment and the end time of the last data segment.

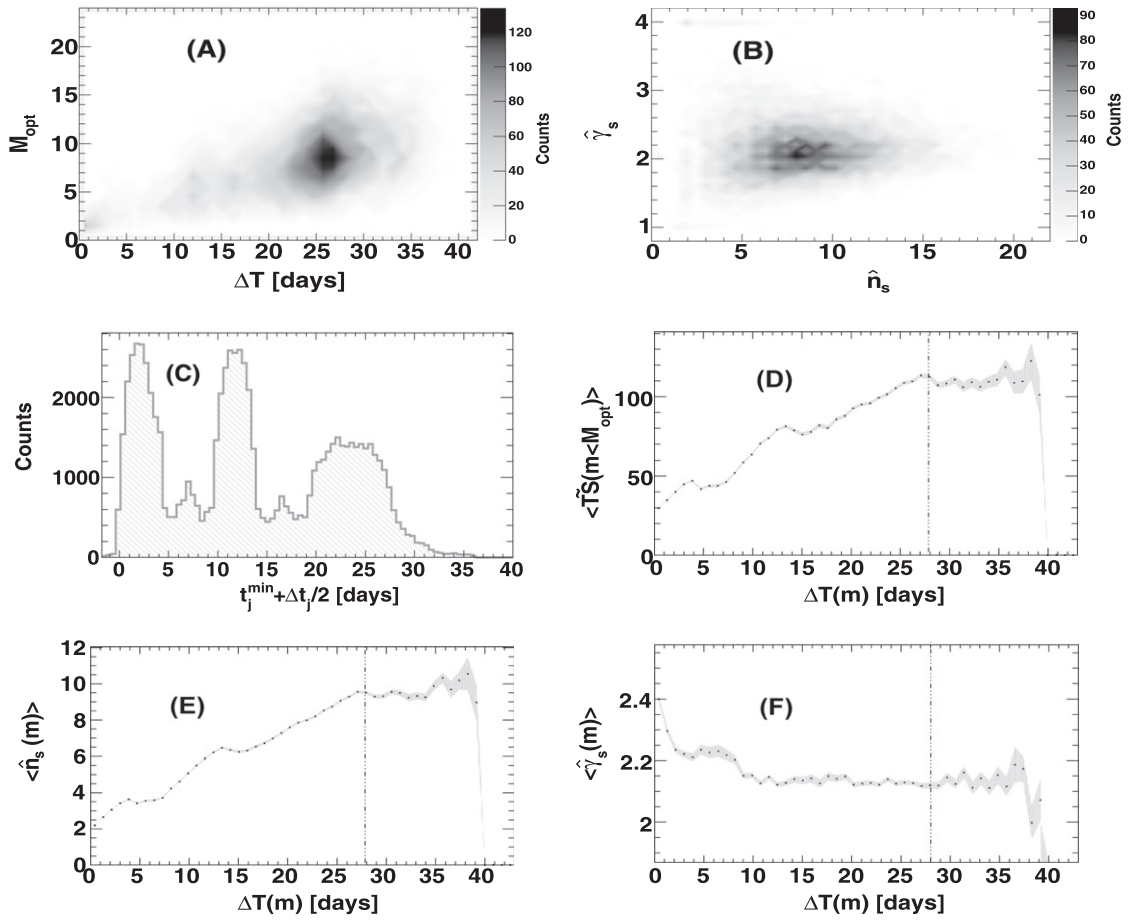

Fig. 7. Example 3: Results of the search for three individual flares separated in time. (A) Distribution of the optimal number of data segments (M_{opt}) as a function of the total flare duration ΔT; (B) The spectral index versus the expected number of signal events; (C) The mean time for each data segments; (D), (E), and (F) The distribution of $<\widetilde{TS}(m)>, <\hat{n}_s(m)>$ and the spectral index $<\hat{\gamma}_s(m)>$, respectively. The vertical dashed line indicates the overall period of enhanced emission (28 days). See the text for more details.

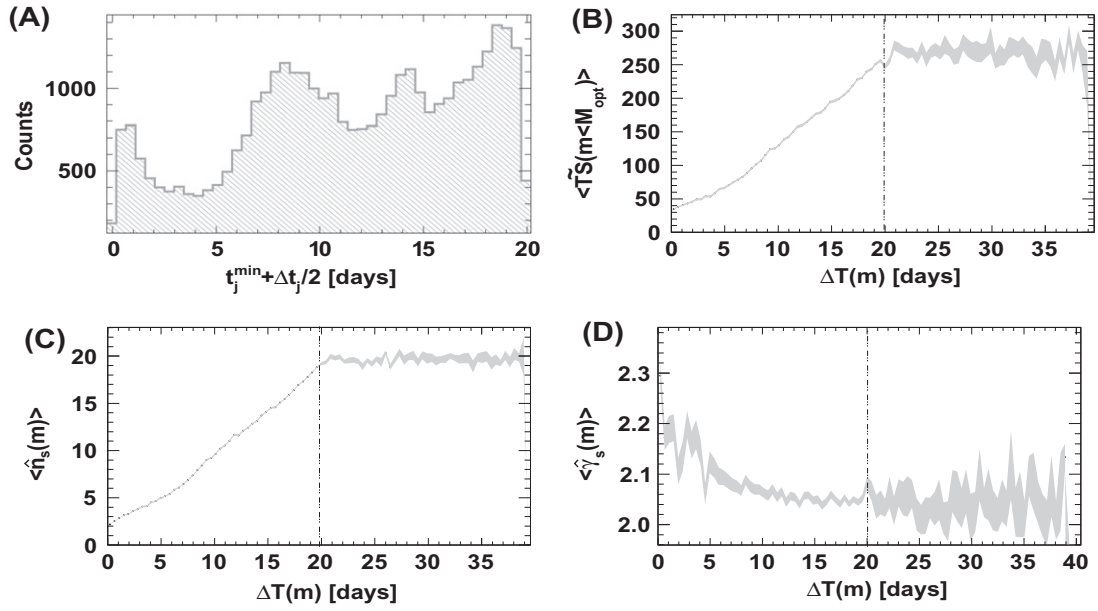

Fig. 8. Example 4: Results of the search, when injected signals events follow a *red-noise* power density spectrum with $\alpha = 2$. (A) The mean time for each data segments; (B), (C), and (D) The distribution of $<\widetilde{TS}(m)>, <\hat{n}_s(m)>$ and the spectral index $<\hat{\gamma}_s(m)>$, respectively. The vertical dashed line indicates the overall period of enhanced emission (20 days). See the text for more details.

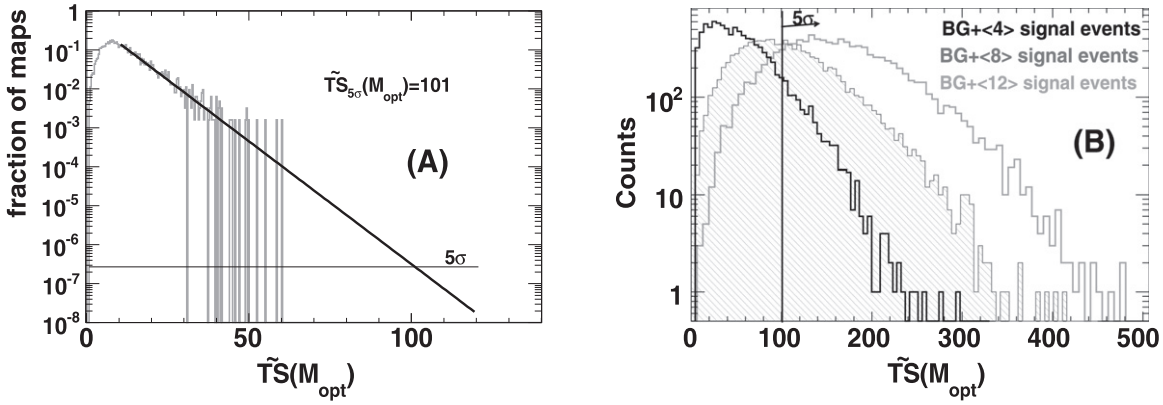

Fig. 9. (A) Probability distribution of the global test statistics $\widetilde{TS}(M_{opt})$ for background-only simulations. The solid line shows an exponential fit to the distribution used to obtain the 5σ threshold for the background only case; (B) Distributions of the test statistic $\widetilde{TS}(M_{opt})$ for background plus signal simulations, where signal events are injected according to a Poisson distribution with mean: 4, 8, 12 signal events, respectively. The vertical line corresponds to the 5σ threshold.

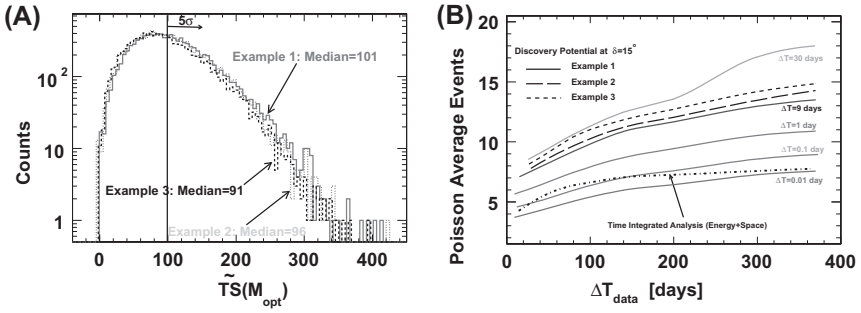

Fig. 10. (A) Distribution of the test statistic $\widetilde{TS}(M_{opt})$ for background plus signal simulations with a Poisson mean of 8 signal events. The results obtained for one flare with duration 9 days (Example 1), two flares with a total duration (including gaps) of 35 days (Example 2) and three weak flares with a total duration of 28 days (Example 3) are compared. The vertical dashed line indicates the 5σ threshold for background only case; (B) Discovery potential as a function of an overall data period ΔT_{data} for one flare with different durations and for two flares and three weak flares. The dashed line shows results of a time-integrated analysis performed in this work with an energy term in the PDF.

according to a Poisson distribution with mean 4, 8 and 12 (the case of Example 1: one flare with duration 9 days). From Fig. 9 (A) we can estimate the $\widetilde{TS}|_{5\sigma}(M_{opt})$ threshold for a 5σexcess in the background only case, which is 101. The 5σ threshold was calculated for a band of ±6°[6] centered at declination 15° and for an overall data period of ΔT_{data} = 40 days. From Fig. 9 (B) we can see that this threshold is passed in 50% of trials when the average number of added signal events is 8. The discovery potential is therefore about 8 events.

In Fig. 10 (A) the global test statistic distribution for the case of Examples 1–3 is shown. The median is 101, 96 and 91, respectively, which means that the number of events required for discovery (assuming a threshold of 101) is 8.0, 8.4 and 8.9. Note that we have a similar number of events required for discovery for Examples 2 and 3 in which signal events are injected over a few flares, but such cases cannot be tested with the method presented in [16].

In Fig. 10 (B) the discovery potential as a function of different overall data periods is shown. The number of events required for discovery as expected depends on the overall data period ΔT_{data} considered. This is because the number of signal-like events increases with time and therefore also leads to a higher 5σ threshold. For example, for an overall data period of 40 days the average number of signal-like events is 5, while it is 43 for a data period of 365 days. Such changes in the number of signal-like events lead to an increase of the 5σ threshold from 101 to 180. As a consequence the number of events needed for discovery increases by about 63%, from 8.0 up to 13 for a flare with a duration of 9 days. Comparing with the results presented in [16] where we need about 9 events for discovery for a method using unknown burst time with energy PDF and one year data period (Fig. 4 in [16]), we see that our method requires about 44% more events for discovery in case all events are injected in one single flare (Example 1). This is because our algorithm stacks also background fluctuations, and thus leads to a higher 5σ threshold than the threshold obtained by a single-source likelihood based method. However, it must be noticed that this comparison is only qualitative, since the signal-to-background ratio which reflect the detector efficiency and signal properties used in both simulations are different. A more quantitative comparison of both two methods have to be achieved on the same simulated data sets. As we also expect, the number of events needed for discovery decreases, when we consider flares with shorter duration. For example, for a flare with duration of 30 days, 1 day, 0.1 day and 0.01 day in average about 9, 6, 5 and 4 events are needed for discovery within ΔT_{data} = 40 days. Note that in this case for flares with shorter duration (below 0.1 days) the number of events is smaller than the number of events for a time-integrated analysis, see Fig. 10 (B) for the method labeled "Time Integrated Analysis (Energy + Space)".

In Fig. 10 (B) the results of calculations for conditions of Examples 2 and 3 are also shown. In general, we see a similar trend i.e. the number of events needed for discovery increases when a larger

[6] Calculations with a larger band (±10°) does not show changes in the 5σ threshold.

overall data period is studied. It is also seen that for Example 2 the number of events for discovery is smaller than for a single flare with similar duration. However, care must be taken in such a comparison because, as we already pointed out before, multiple combinations of individual flares cannot be found by the standard point source search algorithm as proposed in [16]. This is especially true for Example 3. In other words, the performance of the method improves when we study more flares distributed in time, especially if they are weak.

Up to now we also do not exploit the fact that the algorithm provides us information about the number of individual flares distributed in time or even about the number of data segments which compose one flare or a few individual flares separated in time. Using such information, we can calculate a better sensitivity. By dividing the sensitivity by the number of flares or data segments M_{opt}, we can calculate a sensitivity per individual flare or even per segment. For examples presented here (which correspond to signal-like doublets) the number of M_{opt} is about 8 and the number of individual flares is larger than 1, hence the sensitivity can be improved by about the same factor.

5. Summary & conclusion

We have presented a method to search for neutrino flares from point sources without an a priori assumed time structure. The method considers only data segments which contain signal-like doublets, and uses a test-statistic term as their weights in a stacking-like calculation for the global maximum likelihood. We have shown that this method can recover the true values of the source spectral index, the flare duration, and the total number of injected signal events within uncertainties not larger than 10%. In addition, our algorithm provides relevant physics information about the distribution of flares in time and their internal structures. This information can be used to calculate a sensitivity per individual flare, which is usually better than the sensitivity obtained from the other methods.

For standard cases (one "strong" flare), the discovery potential of the method is about 44% worse than the standard point source analysis with unknown duration of the flare. This is because our method stacks all significant background fluctuations in a given period of data and leads to a higher threshold for discovery. However even in such a case, the number of events required for discovery is smaller compared to a time-integrated search as soon as the flare duration is less than a few days. When the number of individual flares analyzed is increased the number of events needed for discovery decreases, especially in the case of a few weak flares distributed over a longer period (from a few days up to 100 days). Such cases of a few weak flares cannot be discovered by the standard point search algorithm [16].

In this work we show that the proposed algorithm can be applied to search for neutrino flares in the data from larger neutrino detector like IceCube. The algorithm presented in this paper is general and in principle could be adopted in any kind of similar analysis. However, as we also have shown, the performance of the method depends on the number of signal-like events in the considered data period. For the detector configuration and data periods studied in this work, the number of signal-like events is usually less than about 50. For data periods or data samples with more signal-like events the performance of the method is worse i.e. the number of events for discovery could be more than shown in Fig. 10 (B). In the case when there are too many data segments containing background events only, the method leads to high threshold for discovery. In other words to transpose the method to other fields, the reduction of the signal-to-noise level is needed. This could be done by considering shortest time intervals, by appling a selection procedure which leads to a lower background level (number of signal-like events less than about (50) or by stacking data segments which have larger multiplicities, for example consecutive quadruplets instead of consecutive doublets. Background fluctuations with larger event multiplicities are less probable, so stacking quadruplets instead of doublets could result lower threshold for discovery.

Acknowledgments

The authors thank A. Kappes and C. Spiering for useful discussions. We acknowledge the support from the Young Investigators Program of the Helmholtz Association.

References

[1] A. Cooper-Sarkar, P. Mertsch, S. Sarkar, The high energy neutrino cross-section in the standard model and its uncertainty, <arXiv:1106.3723>.; A. Cooper-Sarkar, S. Sarkar, Predictions for high energy neutrino cross-sections from the ZEUS global PDF fits, JHEP01 (2008) 075.
[2] B. Baret, V. Van Elewyck, High-energy neutrino astronomy: detection methods and first achievements, Rep. Prog. Phys. 74 (2011) 046902 (For short review on-going multi-messenger programs, see Section 4.5).
[3] M. Kowalski, A. Mohr, Detecting neutrino transients with optical follow-up observations, Astropart. Phys. 27 (6) (2007) 533–538.
[4] A. Franckowiak, C. Akerlof, D.F. Cowen, M. Kowalski, R. Lehmann, T. Schmidt, F. Yuan, for the IceCube Collaboration, Optical follow-up of high-energy neutrinos detected by IceCube, Contributions to the 31st ICRC, Lodz, Poland, July 7–15 (2009).
[5] V. Van Elewyck and on behalf of the ANTARES Collaboration, Multi-messenger programs in ANTARES: status and prospects, Nuclear Instruments and Methods in Physics Research A, 626–627 (SUPPL. 1) (2011) S180–S182.
[6] R. Franke, E. Bernardini for the IceCube collaboration, Neutrino triggered high-energy *gamma*-ray follow-up with IceCube, Contributions to the 31st ICRC, Lodz, Poland, July 7–15 (2009).
[7] J.L. Bazo Alba for the IceCube Collaboration, Search for neutrino flares from point sources with IceCube, Contributions to the 31st ICRC, Lodz, Poland, July 7–15 (2009); <arXiv:0908.4209>.
[8] Protheroe, R.J. et al., Proc. 25th Int. Cosmic Ray Conf. (Durban), 8 (1997) 317.
[9] F. Aharonian et al., Variations of the TeV energy spectrum at different flux levels of Mkn 421 observed with the HEGRA system of Cherenkov telescopes, A& A 393 (2002) 89.
[10] F. Aharonian et al., An exceptional very high energy *gamma*-ray flare of PKS 2155-304, Astrophys. J. 664 (2007) L71–L74.
[11] M. Baker et al. for the IceCube Collaboration, IceCube time-dependent point source analysis using multiwavelength information, Contributions to the 31st ICRC, Lodz, Poland, July 7–15 (2009).
[12] C.D. Dermer, E. Ramirez-Ruiz, T. Le, Correlation of photon and neutrino fluxes in clazars and *gamma*-ray bursts, Astrophys. J. 664 (2007) L67–L70.
[13] K. Satalecka for the IceCube Collaboration, Cluster Search for neutrino flares from pre-defined directions, Contributions to the 30th ICRC, Merida, Mexico, July 3–11, (2007) 115. (<arXiv:0711.0353>).
[14] J. Braun et al., Methods for point source analysis in high energy neutrino telescopes, Astropart. Phys. 29 (2008) 299 (<arXiv:0801.1604>).
[15] <http://mathworld.wolfram.com/HeavisideStepFunction.html>.
[16] J. Braun et al., Time-dependent point source search methods in high energy neutrino astronomy, Astropart. Phys. 33 (2010) 175 (<arXiv:0912.1572>).
[17] R. Abbasi et al., IceCube Collaboration, Time-integrated searches for point-like sources of neutrinos with the 40-string IceCube detector (2010) (<arXiv:1012.2137>).
[18] R. Abbasi et al., IceCube Collaboration, Search for muon neutrinos from *gamma*-ray bursts with the IceCube neutrino telescope, ApJ. 710 (2010) 346 (<arXiv:0907.2227v1>).
[19] M. Tavani et al., Discovery of powerful *gamma*-ray flares from the Crab Nebula 331 (2011) 736.
[20] A.A. Abdo et al., Fermi LAT Collaboration, *Gamma*-ray flares from the Crab Nebula, Science 331 (2011) 739 (<arXiv:1011.3855v1>).
[21] G. Aieli et al., Enhanced TeV gamma ray flux from the Crab Nebula observed, Astronomer's Telegram, <http://www.astronomerstelegram.org/?read=2921>.
[22] A. Lawrence, M.G. Watson, K.A. Pounds, M. Elvis, Low-frequency divergent *X*-ray variability in the Seyfert galaxy NGC4051, Nature 325 (1987) 694–696.
[23] W.H. Press, Flicker noises in astronomy and elsewhere, Comment. Astrophys. 7 (1978) 103.
[24] J. Timmer, M. Konig, On generating power law noise, Astron. Astrophys. 300 (1995) 707–710.